Title

Thermodynamics of Nanoscale Calcium and Strontium Titanate Perovskites

Journal

Journal of the American Ceramic Society, 96(11)

Author

Sahu, Sulata Kumari

Publication Date

2013-08-22

Peer reviewed

J. Am. Ceram. Soc., 1–7 (2013)
DOI: 10.1111/jace.12622

journal

Thermodynamics of Nanoscale Calcium and Strontium Titanate Perovskites

Sulata K. Sahu, Pardha S. Maram, and Alexandra Navrotsky†

Peter A. Rock Thermochemistry Laboratory and NEAT ORU, University of California, Davis, California 95616

The surface enthalpies of nanocrystalline $CaTiO_3$ and $SrTiO_3$ perovskites were determined using high-temperature oxide melt solution calorimetry in conjunction with water adsorption calorimetry. The nanocrystalline samples were synthesized by a hydrothermal method and characterized using powder X-ray diffraction, FTIR spectroscopy, and Brunauer–Emmett–Teller surface area measurements. The integral heats of water vapor adsorption on the surfaces of nanocrystalline $CaTiO_3$ and $SrTiO_3$ are -78.63 ± 4.71 kJ/mol and -69.97 ± 4.43 kJ/mol, respectively. The energies of the hydrous and anhydrous surfaces are 2.49 ± 0.12 J/m^2 and 2.79 ± 0.13 J/m^2 for $CaTiO_3$ and 2.55 ± 0.15 J/m^2 and 2.85 ± 0.15 J/m^2 for $SrTiO_3$, respectively. The stability of the perovskite compounds in this study is discussed according to the lattice energy and tolerance factor approach. The energetics of different perovskites suggest that the formation enthalpy becomes more exothermic and surface energy increases with an increase in ionic radius of the "A" site cation (Ca, Sr, and Ba), or with the tolerance factor. $PbTiO_3$ shows a lower surface energy, weaker water binding, and a less exothermic enthalpy of formation than the alkaline-earth perovskites.

I. Introduction

Perovskites are a versatile group of compounds, and one of the most studied ceramic families, as they form a diversity of materials with various potential applications.[1–5] $CaTiO_3$ and $SrTiO_3$ have attracted considerable attention because they display numerous outstanding physical properties and potential for practical applications.[6–8] These materials are of much interest as dielectrics in ceramic capacitors, in dye-sensitized solar cells, for bone implants, and for use in various other fields.[9–11] Hence, it is important to understand their surface thermodynamic properties, which directly influence their synthesis, processing, sintering, and function. Although theoretical calculations of the surface energy of $CaTiO_3$ and $SrTiO_3$ have been made, no experimentally determined surface energy data have been reported. Over the past decade, high-temperature oxide melt solution calorimetry has been shown to be a powerful and convenient method for studying the surface energies of numerous nanophase oxides.[12–14]

This work presents the formation enthalpies and surface energies of nanoscale perovskite oxides, $CaTiO_3$ and $SrTiO_3$, and compares their energetics to isostructural $BaTiO_3$ and $PbTiO_3$. The samples were synthesized by a hydrothermal method and annealed at different temperatures to produce nanocrystalline powders with different grain sizes. Composition, crystallite size, and surface area were determined using electron microscopy, X-ray diffraction (XRD), and N_2 adsorption experiments. Enthalpies for the hydrous and anhydrous surfaces were determined using high-temperature solution calorimetry and water adsorption microcalorimetry.

II. Experimental Methods

(1) Hydrothermal Synthesis of $ATiO_3$ [A = Ca, Sr] Phases

Nanocrystallites of $ATiO_3$ [A = Ca, Sr] were synthesized using a modified procedure described by Srdić *et al.*[15] (Fig. 1). The synthesis was carried out in two steps. In the first step, $Ti(OC_4H_9)_4$ (98+%; Alfa Aesar, Ward Hill, MA) was dissolved in ethanol (99.5%; Aldrich, St. Louis, MO), in a nitrogen filled glove box. The solution was hydrolyzed with deionized water. The obtained white titania sol was added to a 5N NaOH (EMD Chemicals; Fisher Scientific, Pittsburgh, PA) solution under vigorous stirring to precipitate a titanium hydroxide gel. An aqueous solution containing A^{2+} ions [from $Sr(NO_3)_2$ (99.0%; Alfa Aesar) and $Ca(NO_3)_2{\cdot}4H_2O$ (99.0%; Alfa Aesar)] was slowly added to the prepared slurry under vigorous stirring. Reaction between the titanium hydroxide particles and the corresponding ions was carried out for 1 h at 438 K for $CaTiO_3$ and 453 K for $SrTiO_3$ in a sealed teflon-lined 45 mL autoclave (Parr Instruments, Moline, IL). The obtained powders were washed several times with distilled water to expel sodium ions, and then with absolute ethanol to decrease the degree of agglomeration by removing free water. The washed and dried powders were subjected to heat treatments at various temperatures to obtain materials with varying crystallite size.

(2) Characterization

Powder XRD patterns of the samples were collected using a Bruker AXS D8 Advance diffractometer (Cu$K\alpha$ radiation), (Bruker-AXS Inc., Fitchburg, WI). Data were recorded from 10° to 70° (2θ) at a step size of 0.02° (2θ) and a collection time of 2 s/step. The compositions of the synthesized samples were measured using wavelength dispersive electron probe microanalysis with a Cameca SX100 (Gennevilliers, France) instrument operated at an accelerating voltage of 15 kV, a beam current of 20 nA, and a beam size of 1 μm. Sample homogeneity was analyzed using backscattered electron images. For the microprobe analysis, $CaTiO_3$ and $SrTiO_3$ powders were pelletized and sintered at 1373 K. The sintered pellets were polished and carbon coated. $CaTiO_3$ and $SrTiO_3$ standards were used to measure Sr, Ca, and Ti contents. The sample compositions were calculated from an average of 10 data points per sample.

Surface areas of the nanocrystalline $CaTiO_3$ and $SrTiO_3$ were determined by N_2 adsorption using the Brunauer–Emmett–Teller (BET) method at 77 K. Ten-point nitrogen adsorption isotherms were collected in a relative pressure range of $p/p^0 = 0.05$–0.3 (where, p^0 = saturation pressure) using a Micromeritics ASAP 2020 surface area and porosity analyzer (Micromeritics Instrument Corp., Norcross, GA). Before analysis, the samples were degassed under vacuum at 300°C for 2 h. The uncertainties in the BET surface area measurements were propagated from fitting a straight line to $1/[Q(p^0/p_1)]$ (Q = quantity adsorbed, mmol/g) versus p/p^0

T. Vanderah—contributing editor

Manuscript No. 33323. Received June 5, 2013; approved August 22, 2013.
†Author to whom correspondence should be addressed. e-mail: anavrotsky@ucdavis.edu

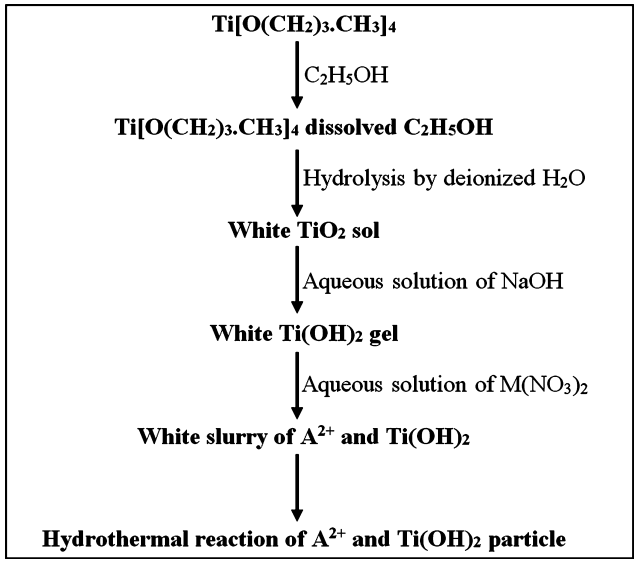

Fig. 1. Experimental procedures for the synthesis of $ATiO_3$ ($A = Sr^{2+}$ and Ca^{2+}).

using the Micromeritics software. The total amount of water (chemisorbed and physisorbed) on the nanocrystalline samples was determined on a set of five samples, each 10–15 mg, by thermogravimetric analysis using a Netzsch STA 449 system (Netzsch GmbH, Selb, Germany). The sample was heated in a platinum crucible from 303 to 1173 K in an oxygen atmosphere at 10 K/min. A buoyancy correction was made by subtracting the baseline collected by running an identical Differential Thermal Analysis/Differential Scanning Calorimetry (TGA/DSC) scan with an empty platinum crucible. The water content was determined from the TGA weight-loss curve. The gases that evolved during the thermal analysis were analyzed by infrared spectroscopy (IR) using a Bruker Equinox 55 FTIR spectrometer (range 400–4000 cm^{-1}) coupled to the TGA/DSC by a transfer line heated to 423 K.

(3) Water Adsorption Calorimetry

Nanoparticles are very hygroscopic, and not all surface water can be removed without sample coarsening. Hence, it is important to account for the chemically and physically adsorbed water to deduce accurate surface enthalpies of both the hydrated and anhydrous surfaces.[16] The enthalpy of water vapor adsorption was measured at 298 K using a Setaram Calvet-type Sensys calorimeter (Setaram Instruments, Caluire, France) coupled with the Micromeritics ASAP 2020 instrument. The calorimeter was calibrated against the enthalpy of fusion of gallium metal. The instrumental design is described in detail elsewhere.[17] This technique enables precise gas dosing, volumetric detection of the amount of adsorbed water, and simultaneous measurement of the heat effect. The sample was placed in one side of a specially designed silica glass fork tube so that it could fit into the twin chambers of the microcalorimeter, with the empty tube serving as a reference. The experiment comprised three steps. In the first step, the sample was degassed under vacuum (<0.3 Pa) for 3 h at 573 K for $CaTiO_3$ and 673 K for $SrTiO_3$. The second step involved measurement of the free volume of the sample tube with helium, and the BET surface area of the sample by nitrogen adsorption. In the third step, a water adsorption calorimetry experiment was programmed in incremental dose mode to provide ~2 μmol of H_2O/nm^2 per dose. The surface area of each sample used was 2 m^2. The integral enthalpy of water adsorption and surface coverage were calculated from an average of three experiments. A correction from a blank run was applied to account for water adsorbed onto the instrument manifold, and onto the walls of the sample tube.

(4) High-Temperature Oxide Melt Solution Calorimetry

The drop solution enthalpies of $CaTiO_3$ and $SrTiO_3$ samples of different crystallite sizes were measured in a custom-made isoperibol Tian-Calvet twin microcalorimeter (University of California, Davis, CA) described previously.[12,13] The calorimeter assembly was flushed with oxygen at 43 mL/min. Oxygen was bubbled through the solvent at 4.5 mL/min to aid dissolution and maintain oxidizing conditions. Pellets of approximately 5 mg were loosely pressed, weighed, and dropped from room temperature into $3Na_2O{\cdot}4MoO_3$ molten solvent at 975 K. Measurements were repeated 8–10 times for each sample to achieve statistically reliable data. The calorimeter was calibrated against the heat content of 5 mg pellets of high purity α-Al_2O_3 (99.997%; Alfa Aesar) dropped into an empty crucible. Before the drop solution experiments, all samples were equilibrated at 298 ± 1 K and 50 ± 5% humidity in the calorimetry laboratory, and the water contents of these equilibrated samples were determined by weight-loss measurements after annealing at 1173 K for 14 h in air. Surface energy calculations from high-temperature drop solution calorimetry data were completed according to methods in earlier studies.[17–19]

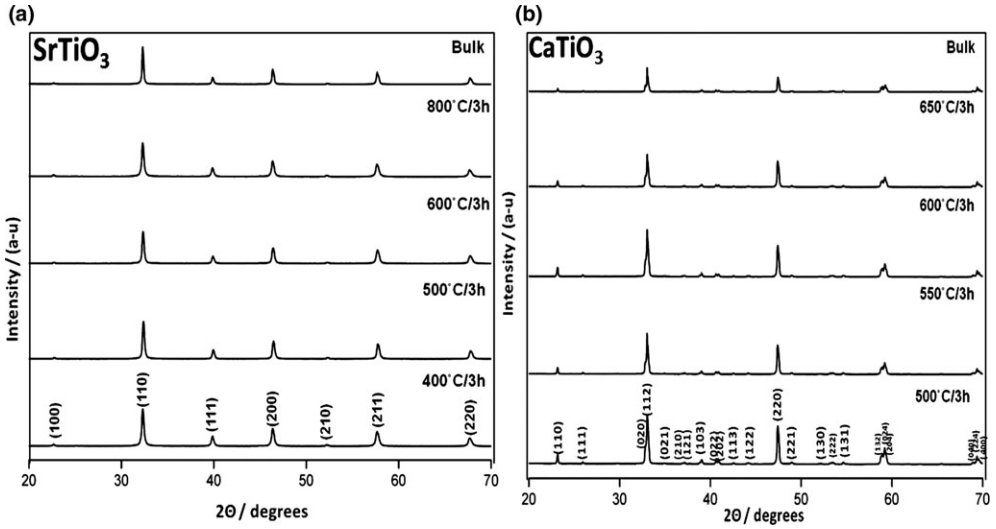

Fig. 2. (a) X-ray diffraction patterns of $SrTiO_3$ annealed at various temperature. All patterns are indexed based on JCPDS no. 86-0179. (b) XRD patterns of $CaTiO_3$ annealed at various temperature. All patterns are indexed based on JCPDS no. 86-1393.

Table I. Summary of Data used for the Calculation of Surface Enthalpies of $CaTiO_3$ and $SrTiO_3$

Temp. (K)	XRD crystallite size (nm)	BET SA (m^2/mol)	H_2O (mol)			ΔH_{ds} k/Jmol in $2Na_2O{\cdot}4MoO_3$[¶]		
			n^t(total)[†]	x (chemi)[§]	y ($n - x$), physi	$ATiO_3{\cdot}nH_2O$	Hydrous	Anhydrous
$CaTiO_3$								
773/3 h	54.3 ± 3.8	1739 ± 49	0.055 ± 0.001	0.011 ± 0.006	0.044 ± 0.006	51.25 ± 0.92(9)	47.49 ± 0.92	47.09 ± 0.93
823/3 h	64.8 ± 2.5	1113 ± 28	0.039 ± 0.001	0.007 ± 0.003	0.032 ± 0.003	51.49 ± 0.56(9)	48.78 ± 0.56	48.52 ± 0.57
873/3 h	66.6 ± 1.3	913 ± 22	0.032 ± 0.009	0.006 ± 0.002	0.026 ± 0.009	51.63 ± 0.72(8)	49.45 ± 0.72	49.27 ± 0.72
923/3 h	72.1 ± 2.9	574 ± 16	0.025 ± 0.002	0.006 ± 0.001	0.019 ± 0.003	52.05 ± 0.62(8)	50.33 ± 0.62	50.20 ± 0.62
Bulk	>1000	–	–			51.66 ± 0.99 (9)		
$SrTiO_3$								
673/3 h	30.9 ± 2.3	4613 ± 23	0.127 ± 0.018	0.047 ± 0.022	0.080 ± 0.029	51.06 ± 0.50(9)	42.29 ± 0.52	40.44 ± 0.61
773/3 h	35.0 ± 1.8	3923 ± 35	0.102 ± 0.009	0.040 ± 0.02	0.063 ± 0.02	51.82 ± 0.61(8)	44.75 ± 0.62	43.60 ± 0.67
873/3 h	41.9 ± 2.2	3272 ± 17	0.075 ± 0.008	0.033 ± 0.016	0.041 ± 0.178	50.64 ± 0.75(8)	45.49 ± 0.76	44.53 ± 0.79
1073/3 h	44.6 ± 3.1	1829 ± 44	0.029 ± 0.004	0.019 ± 0.009	0.010 ± 0.010	51.22 ± 0.49(8)	49.23 ± 0.49	48.69 ± 0.51
Bulk	>1000	–	–			54.71 ± 0.92 (8)		

[†]Total amount of water in moles measured by gravimetric analysis.
[§]Chemi adsorbed water in moles measured using water adsorption calorimetry.
[¶]Mean values from the number of experiments given in parentheses; uncertainties are calculated as two standard deviations of the mean.

III. Results and Discussion

(1) Structural Characterization

Figure 2 shows the powder XRD patterns of $SrTiO_3$ and $CaTiO_3$ samples prepared by a hydrothermal method followed by annealing at different temperatures. Annealing $SrTiO_3$ at 673 K for 3 h yielded crystallites of $SrTiO_3$ in a single phase without any impurities. Similarly, annealing $CaTiO_3$ at 773 K for 3 h resulted in pure $CaTiO_3$ nanocrystals. The crystallite sizes from whole pattern profile refinement are given in Table I. According to the microprobe analysis, the samples are stoichiometric within experimental error, namely, $Sr_{0.994 \pm 0.002}Ti_{1.006 \pm 0.001}O_{3.006 \pm 0.003}$ and $Ca_{0.993 \pm 0.006}Ti_{1.007 \pm 0.004}O_{3.007 \pm 0.005}$. No secondary phases were observed on the backscattered electron images of the sintered samples. The analyzed compositions were used in the thermochemical calculations.

The BET surface area (BET SA) of the nanocrystalline $SrTiO_3$ samples diminished from ~5 × 10^3 to ~2 × 10^3 m^2/mol upon increasing the annealing temperature from 673 to 1073 K. For the $CaTiO_3$ samples, BET SA decreased from ~2 × 10^3 to ~0.6 × 10^3 m^2/mol upon increasing the annealing temperature from 773 to 923 K (Table I). Based on the TG traces, all samples show continuous weight loss to ~723 K. The FTIR spectra of the evolved gases show only the characteristic IR bands of water vapor.

(2) Energetics of Water Vapor Adsorption

Figure 3 shows the variation in total water content, "n" in $ATiO_3{\cdot}nH_2O$, measured by weighing the samples before and after heat treatment, with surface area. The adsorption enthalpies for individual doses (differential enthalpies of adsorption, see Fig. 4) become less exothermic with successive water doses, and eventually reach the enthalpy of bulk water condensation (−44.0 ± 0.1 kJ/mol). The total water content, n, consists of two parts: $n = x + y$; here, x is the amount of chemisorbed water, characterized by adsorption enthalpies more negative than the enthalpy of water vapor condensation, and y is the amount of physisorbed water, characterized by adsorption enthalpies equal to the enthalpy of water vapor condensation (Table I).

For $SrTiO_3$ and $CaTiO_3$, the chemisorbed water content amounts to a coverage of 6.78 ± 0.41 and 5.23 ± 0.14 H_2O/nm^2, respectively. The integral enthalpy, which is the sum of the differential enthalpies of adsorption divided by the total amount of water up to the given coverage, gives the average total adsorption enthalpy. The integral enthalpies of water

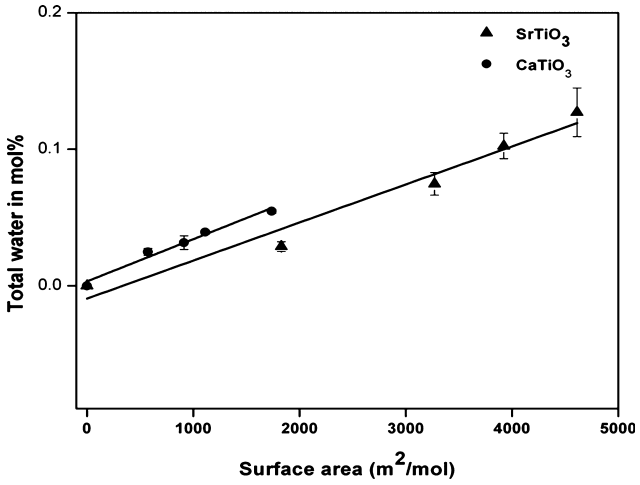

Fig. 3. Total water content obtained from weight loss experiments for different samples of $SrTiO_3$ and $CaTiO_3$ versus BET surface area. The x-axis error bars are not visible since they are smaller than the symbol size.

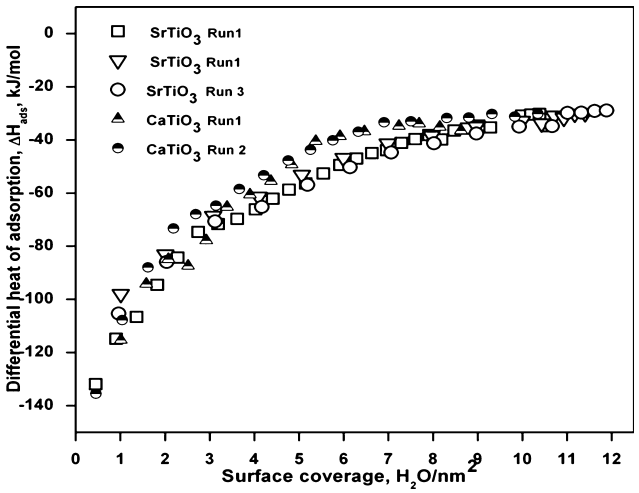

Fig. 4. Differential enthalpy of H_2O adsorption on the surface of $SrTiO_3$ and $CaTiO_3$ nanocrystals versus water coverage.

Table II. Thermochemical Cycle used for Water Correction for Energy of (A) Hydrous Surface and (B) Anhydrous Surface

(A) Hydrous surface	
$ATiO_3{-}nH_2O$ (solid, 298 K) → $ATiO_3$ (soln., 973 K) + nH_2O (gas, 973 K)	$\Delta H_1 = \Delta H_{ds}$
nH_2O (gas, 973 K) → nH_2O (gas, 298 K)	$\Delta H_2 = n\ (-25.1 \pm 0.1)$ kJ/mol[25]
nH_2O (gas, 298 K) → nH_2O (liq., 298 K)	$\Delta H_3 = n\ (-44.0 \pm 0.1)$ kJ/mol[25]
$ATiO_3$(solid, 298 K) → $ATiO_3$(soln., 973 K)	$\Delta H_4 = \Delta H_{ds.corr} = \Delta H_1 + \Delta H_2 + \Delta H_3$
(B) Anhydrous surface	
$ATiO_3$ $(x + y)$ H_2O (nano, 298 K) = $ATiO_3$ (soln., 973 K) + $(x + y)$ H_2O (gas, 973 K)	$\Delta H_1 = \Delta H_{ds}$
$(x + y)$ H_2O (gas, 973 K) = $(x + y)$ H_2O (gas, 298 K)	$\Delta H_2 = (x + y)\ (-25.1 \pm 0.1)$ kJ/mol[25]
(y) H_2O (gas, 298 K) = (x) H_2O (liq., 298 K)	$\Delta H_3 = y\ (-44.0 \pm 0.1)$ kJ/mol[25]
(x) H_2O (gas, 298 K) = (y) H_2O (liq., 298 K)	$\Delta H_5 = x\ (\Delta H_{integral}\ H_2O)$ kJ/mol
$ATiO_3$(nano, 298 K) = $ATiO_3$ (soln. $3Na_2O{\cdot}4MoO_3$ at 973 K)	$\Delta H_6 = \Delta H_{ds.corr} = \Delta H_1 + \Delta H_2 + \Delta H_3 + \Delta H_5$

Soln. means dissolved in $3Na_2O{\cdot}4MoO_3$.
where x = moles chemisorbed water and y = moles physisorbed water.

chemisorptions for $SrTiO_3$ and $CaTiO_3$ are -69.97 ± 4.43 and -78.63 ± 4.71 kJ/mol, respectively, calculated as the average from two experiments. The integral enthalpies of water chemisorption for $CaTiO_3$ and $SrTiO_3$ for the same coverage are comparable, suggesting that the chemical bonding of water to the surface atoms of $CaTiO_3$ and $SrTiO_3$ is similar.

(3) Calculation of Surface and Formation Enthalpy

The enthalpies of drop solution for the entire set of $CaTiO_3$ and $SrTiO_3$ samples with varying surface areas are given in Table I. The difference between the enthalpy of drop solution, ΔH_{ds}, of bulk and nanosamples, corrected for water content, arises from the surface energy term (γ*SA, where SA is the surface area and γ is the surface enthalpy):

$$\Delta H_{ds}(\text{nano}) = \Delta H_{ds}(\text{bulk}) + \gamma * SA \quad (1)$$

A linear variation of ΔH_{ds} with surface area, as seen in this work, suggests a surface energy independent of particle size in the range studied. As all nanocrystalline samples have hydrated surfaces, the ΔH_{ds} values were corrected for water content following the procedures described in detail previously.[20–24] When the heat content of bulk water is used for this correction, the surface energy obtained characterizes the energetics of the hydrated surface.[25] The thermochemical cycle used for water correction is given in Table II. Figure 5 shows a linear fit of the corrected drop solution enthalpy of different nanocrystalline samples versus SA. The slope corresponds to the enthalpy of the hydrated surface, and is 2.55 ± 0.15 J/m^2 for $SrTiO_3$ and 2.49 ± 0.12 J/m^2 for $CaTiO_3$. One can calculate the enthalpy of the anhydrous surface by applying a water correction, including the actual interaction of water with the surface, to the directly measured water adsorption enthalpy using the thermochemical cycle in Table II and the water adsorption data in Table I. The slope of this fit (see Fig. 5) corresponds to the enthalpy of the anhydrous surface, 2.85 ± 0.15 J/m^2 for $SrTiO_3$ and 2.79 ± 0.12 J/m^2 for $CaTiO_3$. The enthalpy of the anhydrous surface is generally the appropriate value to compare to computational results.

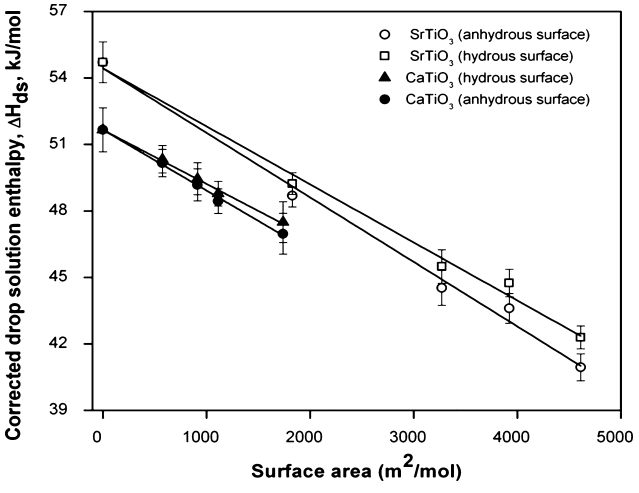

Fig. 5. Water corrected drop solution enthalpies of $SrTiO_3$ and $CaTiO_3$ versus surface area.

Table III shows the thermochemical cycle used to determine the enthalpies of formation of $SrTiO_3$ and $CaTiO_3$. For this, the enthalpy of drop solution of SrO and CaO in $3Na_2O{\cdot}4MoO_3$ at 975 K was taken from Refs. [26–28] whereas the ΔH_{ds} of $SrTiO_3$ and $CaTiO_3$ were determined in this study. The obtained enthalpy of formation from corresponding oxides, $\Delta H_{f,ox}$, is -131.54 ± 3.44 kJ/mol for $SrTiO_3$ and -83.76 ± 2.72 kJ/mol for $CaTiO_3$. The enthalpy of formation from oxides ($\Delta H_{f,ox}$) and enthalpy of drop solution (ΔH_{ds}) of $SrTiO_3$ and $CaTiO_3$ are consistent with previous reports.[27–30]

The surface enthalpies for various planes of $SrTiO_3$ and $CaTiO_3$ have been calculated by density functional theory (Table IV).[31–38] Our experimentally measured values are ~50% higher than the theoretical ones, which may be because the measured surface energy is an average over many planes, edges, kinks, steps, and other surface defects. However, theoretical surface energies are calculated for idealized and generally perfect crystals (relaxed or unrelaxed, but uniform). The discrepancy may also point to some deficiencies in the computations, since an important role of experimental data is to benchmark such calculations.

(4) Comparison of Surface Energies of $SrTiO_3$, $CaTiO_3$, $BaTiO_3$, and $PbTiO_3$

As indicated in Table V, the chemisorbed water coverage of all four studied perovskites ($BaTiO_3$ and $PbTiO_3$)[39] are similar. However, the integral enthalpy of water vapor adsorption (ΔH_{ads}) for $PbTiO_3$ is less exothermic than the values for the other $ATiO_3$ perovskites (A = Ca, Sr, Ba), indicating that water is bound less strongly to the surface of $PbTiO_3$. Hence, the surface of $PbTiO_3$ is less hydrophilic than those of the alkaline-earth titantate perovskites. The reduced hydrophilicity of the $PbTiO_3$ surface may reflect its lone pair of electrons, which perhaps interfere with the bonding of H_2O or OH^- to the surface.[40] Analogous behavior was seen in the isostructural rutile oxides, SnO_2 and TiO_2, with SnO_2 having lower surface energy and lower water adsorption enthalpy than TiO_2.[22,41]

Table III. Thermochemical Cycles used for the Calculation of Formation Enthalpies of $ATiO_3$ (A: Sr^{2+} and Ca^{2+})

AO (solid, 298 K) = AO (soln., 973 K)	ΔH_I[27]
TiO_2(solid, 298 K) = TiO_2 (soln., 973 K)	ΔH_{II}[28]
$ATiO_3$ (solid, 298 K) = AO (soln., 973 K) + TiO_2(soln., 973 K)	$\Delta H_{III} = \Delta H_{ds}$
AO (solid, 298 K) + TiO_2 (xl, 298 K) = $ATiO_3$ (xl, 298 K)	$\Delta H_{IV} = \Delta H_{f,ox} = \Delta H_I + \Delta H_{II} - \Delta H_{III}$

Table IV. Surface Enthalpy of $SrTiO_3$ and $CaTiO_3$ Compared with Theoretical Studies

		Surface energy (J/m^2)			
		$SrTiO_3$		$CaTiO_3$	
Reference	Surfaces	TiO_2 termination	SrO termination	TiO_2 termination	CaO termination
This work	Experimental	2.85 ± 0.15		2.79 ± 0.13	
31	(001)	1.29	1.21	1.18	1.00
32	(001)	1.32	1.29	1.33	1.06
33	(001)	1.31		1.418	
34	(001)	1.03	1.01	1.01	0.81
36	(001)	1.30	1.25	–	
37	(001)	1.37	1.21	1.20	1.00
38	(001)	1.43	1.39	–	

Table V. Water Adsorption Enthalpy and Surface Energy of $SrTiO_3$, $CaTiO_3$, and Comparison with $PbTiO_3$ and $BaTiO_3$

Compounds	$PbTiO_3$[39]	$CaTiO_3$	$SrTiO_3$	$BaTiO_3$[39]
Formation enthalpy from oxides (kJ/mol)[30]	−31.1 ± 4.1	−80.9 ± 2.3	−135.1 ± 2.2	−152.3 ± 4.0
Tolerance factor	1.11	0.97	1.09	1.15
ΔE_M (electrostatic energy difference) (kJ/mol)	58	−322	−225	−27
ΔE_N (nonelectrostatic energy difference) (kJ/mol)	−89	241	90	−125
Chemisorbed coverage (H_2O/nm^2)	6.2 ± 0.2	5.23 ± 0.14	6.78 ± 0.41	5.2 ± 0.7
Integral enthalpy at chemisorbed coverage ΔH_{ads}(kJ/mol)	−62 ± 4	−78.63 ± 4.71	−69.97 ± 4.43	−79 ± 5
Surface energy, hydrous (J/m^2)	1.97 ± 0.67	2.49 ± 0.12	2.55 ± 0.15	3.69 ± 0.22
Surface energy, anhydrous (J/m^2)	1.11 ± 0.23	2.79 ± 0.13	2.85 ± 0.15	3.99 ± 0.28

The stability of perovskite compounds was discussed by Takayama-Muromachi and Navrotsky[42] using a lattice energy approach. The internal energy of an ionic crystal can be separated into two terms:

$$E = E_M + E_N \quad (2)$$

where E_M is the electrostatic (Madelung) energy, and E_N includes all other interaction energies, among which the repulsive energy gives the largest contribution. For the reaction:

$$AO + BO_2 = ABO_3(\text{perovskite}) \quad (3)$$

the internal energy difference between the product and the reactant is essentially the same as the formation enthalpy of the perovskites from their binary oxide components. Therefore, the formation enthalpy from the oxide components can be represented as

$$\Delta H_f^0 = \Delta E = \Delta E_M + \Delta E_N \quad (4)$$

where ΔE_M and ΔE_N are the electrostatic energy difference and the nonelectrostatic energy difference between the product and the reactants, respectively. More negative value of ΔE_M, during the perovskite formation from their constituent oxides indicates the perovskite formation is more favorable. In the present case, ΔE_M is negative for all perovskites except $PbTiO_3$. Similarly, positive values of ΔE_N suggest that repulsive interactions increase on formation of the perovskites from their constituent oxides and a positive ΔE_N during the perovskite formation from their constituent oxides implies destabilization. The variation of ΔE_N with the tolerance factor is shown in Fig. 6, indicating that the repulsive energy change becomes more favorable with an increase in the tolerance factor, t, given by:

$$t = (r_A + r_O)/\sqrt{2}(r_B + r_O) \quad (5)$$

Here, r_A, r_B, and r_O refer to the ionic radii of A^{2+}, B^{4+}, and O^{2-}, respectively. An A^{2+} coordination of 8 is assumed for Ca, and 12 for Sr, Pb, and Ba.[43]

Figure 7 represents the relation between formation enthalpies and surface energy for various perovskites. The surface energy increases as the formation enthalpy becomes more exothermic. Similarly, Fig. 8 shows the water adsorption enthalpy as a function of surface enthalpy. With an increase in surface enthalpy, the water adsorption enthalpy becomes more exothermic, suggesting that surfaces become more hydrophilic with an increase in their surface energy, a trend seen in other oxides.[39] Thus, the more ionic the perovskite, the more stable it is, the higher is its surface energy, and the more tightly it binds water.

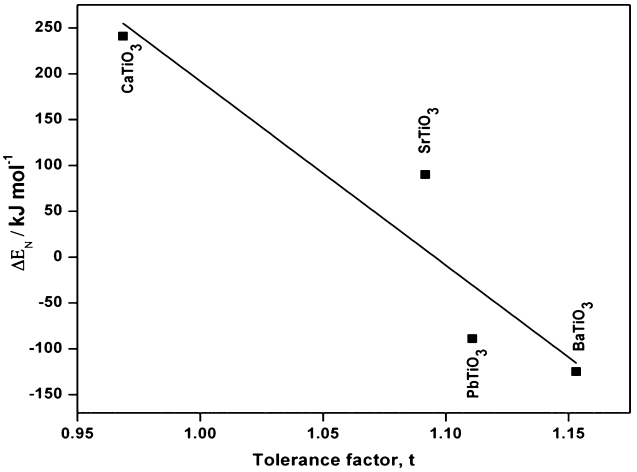

Fig. 6. Relationship between nonelectrostatic energy and tolerance factor.

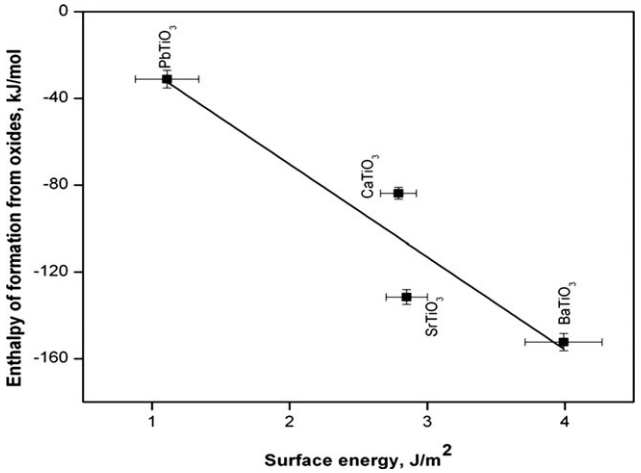

Fig. 7. Enthalpy of formation of perovskites from oxides versus surface enthalpy for the anhydrous surfaces.

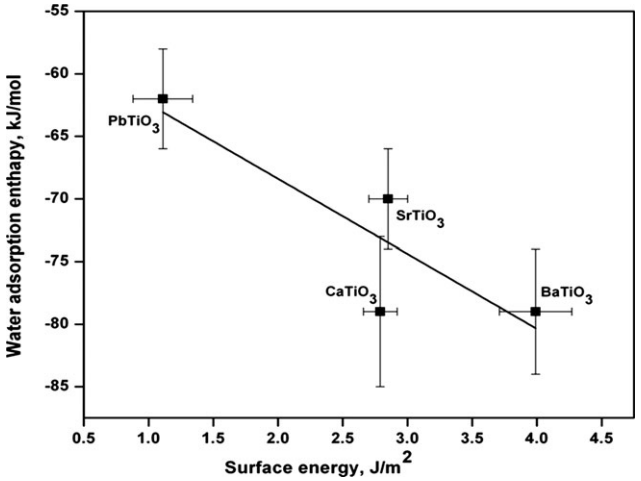

Fig. 8. Water adsorption enthalpy of $ATiO_3$ perovskites with A = Ca, Sr, Ba, and Pb versus surface enthalpy for anhydrous surface.

IV. Conclusions

Nanocrystalline perovskite oxides, $CaTiO_3$ and $SrTiO_3$, were synthesized by a modified hydrothermal method with BET SAs ranging from 4 to 25 m^2/g. Using water adsorption calorimetry and high-temperature oxide melt solution calorimetry, we determined the surface enthalpies for the hydrous and anhydrous surfaces of $CaTiO_3$ and $SrTiO_3$ to be 2.49 ± 0.12 and 2.55 ± 0.15, and 2.79 ± 0.13 and 2.85 ± 0.15 J/m^2, respectively. The enthalpies of water vapor adsorption on the surfaces of nanocrystalline $CaTiO_3$ and $SrTiO_3$ were found to be -78.63 ± 4.71 and -69.97 ± 4.43 kJ/mol, with total water coverages of 5.23 ± 0.14 and 6.78 ± 0.41 H_2O/nm^2, respectively. The water adsorption enthalpies and formation enthalpies of perovskites become more exothermic and their surface energies increase in the order Pb, Ca, Sr, and Ba.

Acknowledgment

This research has received funding from the US Department of Energy, grant no. DE-FG02-05ER15667.

References

[1]N. Izyumskaya, Y. I. Alivov, S. J. Cho, H. Morkoc, H. Lee, and Y. S. Kang, "Processing, Structure, Properties, and Applications of PZT Thin Films"; pp. 111–202 in *Crit. Rev. Solid State Mater. Sci.*, Vol. 32, Taylor & Francis, Inc., London, 2007.

[2]A. Navrotsky, "Thermodynamics of Solid Electrolytes and Related Oxide Ceramics Based on the Fluorite Structure," *J. Mater. Chem.*, **20** [47] 10577–87 (2010).

[3]J. Linton, A. Navrotsky, and Y. Fei, "The Thermodynamics of Ordered Perovskites on the $CaTiO_3$–$FeTiO_3$ Join," *Phys. Chem. Miner.*, **25** [8] 591–6 (1998).

[4]R. E. Newnham and L. E. Cross, "Ferroelectricity: The Foundation of a Field from Form to Function," *MRS Bull.*, **30** [11] 845–8 (2005).

[5]Y. Yamashita, K. Harada, and S. Saitoh, "Recent Applications of Relaxor Materials," *Ferroelectrics*, **219** [14] 665–72 (1998).

[6]K. C. Chiang, C. C. Huang, G. L. Chen, W. J. Chen, H. L. Kao, Y. H. Wu, A. Chin, and S. P. McAlister, "High-Performance $SrTiO_3$ MIM Capacitors for Analog Applications," *IEEE Trans. Electron Devices*, **53** [9] 2312–9 (2006).

[7]T. Wolfram, E. A. Kraut, and F. J. Morin, "D-Band Surface States on Transition-Metal Perovskite Crystals .1. Qualitative Features and Application to $SrTiO_3$," *Phys. Rev. B*, **7** [4] 1677–94 (1973).

[8]K. X. Jin, Y. F. Li, Z. L. Wang, H. Y. Peng, W. N. Lin, A. K. K. Kyaw, Y. L. Jin, K. J. Jin, X. W. Sun, C. Soci, and T. Wu, "Tunable Photovoltaic Effect and Solar Cell Performance of Self-Doped Perovskite $SrTiO_3$," *AIP Adv.*, **2** [4] 042131, 9pp (2012).

[9]M. Yashima and M. Tanaka, "Performance of a New Furnace for High-Resolution Synchrotron Powder Diffraction up to 1900 K: Application to Determine Electron Density Distribution of the Cubic $CaTiO_3$ Perovskite at 1674 K," *J. Appl. Crystallogr.*, **37**, 786–90 (2004).

[10]C. Gargori, R. Galindo, S. Cerro, M. Llusar, A. Garcia, J. Badenes, and G. Monros, "Ceramic Pigments Based on Chromium and Vanadium Doped $CaTiO_3$ Perovskite Obtained by Metal Organic Decomposition (MOD)," *Bol. Soc. Esp. Ceram. Vidrio*, **51** [6] 343–52 (2012).

[11]T. R. S. Prasanna and A. Navrotsky, "Energetics in the Brownmillerite Perovskite Pseudobinary $Ca_2Fe_2O_5$–$CaTiO_3$," *J. Mater. Res.*, **9** [12] 3121–4 (1994).

[12]A. Navrotsky, "Thermochemistry of New Technologically Important Inorganic Materials," *MRS Bull.*, **22** [5] 35–41 (1997).

[13]A. Navrotsky, "Progress and New Directions in High Temperature Calorimetry Revisited," *Phys. Chem. Miner.*, **24** [3] 222–41 (1997).

[14]M. P. Saradhi, S. V. Ushakov, and A. Navrotsky, "Fluorite-Pyrochlore Transformation in $Eu_2Zr_2O_7$-Direct Calorimetric Measurement of Phase Transition, Formation and Surface Enthalpies," *RSC Adv.*, **2** [8] 3328–34 (2012).

[15]V. V. Srdić, R. Djenadic, M. Milanovic, N. Pavlovic, I. Stijepovic, L. M. Nikolic, E. Moshopoulous, K. Giannakopoulos, J. Dusza, and K. Maca, "Direct Synthesis of Nanocrystalline Oxide Powders by Wet-Chemical Techniques," *Process. Appl. Ceram.*, **4** [3] 127–34 (2010).

[16]R. H. R. Castro and D. V. Quach, "Analysis of Anhydrous and Hydrated Surface Energies of Gamma-Al_2O_3 by Water Adsorption Microcalorimetry," *J. Phys. Chem. C*, **116** [46] 24726–33 (2012).

[17]S. V. Ushakov and A. Navrotsky, "Direct Measurements of Water Adsorption Enthalpy on Hafnia and Zirconia," *Appl. Phys. Lett.*, **87** [16] 164103, 3pp (2005).

[18]S. Hayun, T. Y. Shvareva, and A. Navrotsky, "Nanoceria – Energetics of Surfaces, Interfaces and Water Adsorption," *J. Am. Ceram. Soc.*, **94** [11] 3992–9 (2011).

[19]G. C. C. Costa, S. V. Ushakov, R. H. R. Castro, A. Navrotsky, and R. Muccillo, "Calorimetric Measurement of Surface and Interface Enthalpies of Yttria-Stabilized Zirconia (YSZ)," *Chem. Mater.*, **22** [9] 2937–45 (2010).

[20]T. J. Park, A. A. Levchenko, H. J. Zhou, S. S. Wong, and A. Navrotsky, "Shape-Dependent Surface Energetics of Nanocrystalline TiO_2," *J. Mater. Chem.*, **20** [39] 8639–45 (2010).

[21]P. Zhang, V. Xu, A. Navrotsky, J. S. Lee, S. T. Kim, and J. Liu, "Surface Enthalpies of Nanophase ZnO with Different Morphologies," *Chem. Mater.*, **19** [23] 5687–93 (2007).

[22]A. A. Levchenko, G. S. Li, J. Boerio-Goates, B. F. Woodfield, and A. Navrotsky, "TiO_2 Stability Landscape: Polymorphism, Surface Energy, and Bound Water Energetics," *Chem. Mater*., **18** [26] 6324–32 (2006).

[23]W. Zhou, S. V. Ushakov, T. Wang, J. G. Ekerdt, A. A. Demkov, and A. Navrotsky, "Hafnia: Energetics of Thin Films and Nanoparticles," *J. Appl. Phys*., **107** [12] 123514, 7pp (2010).

[24]A. V. Radha, O. Bomati-Miguel, S. V. Ushakov, A. Navrotsky, and P. Tartaj, "Surface Enthalpy, Enthalpy of Water Adsorption, and Phase Stability in Nanocrystalline Monoclinic Zirconia," *J. Am. Ceram. Soc*., **92** [1] 133–40 (2009).

[25]R. A. Robie, B. S. Hemingway, and J. R. Fisher, "*Thermodynamic Properties of Minerals and Related Substances at 298.15 K and 1 Bar (105 Pascals) Pressure and at Higher Temperatures*"; U. S. Geological Survey Bulletin 2131, U.S. Geological Survey, Reston, VA, 1995.

[26]H. H. Cheng and A. Navrotsky, "Energetics of Magnesium, Strontium, and Barium Doped Lanthanum Gallate Perovskites," *J. Solid State Chem*., **177** [1] 126–33 (2004).

[27]K. B. Helean, A. Navrotsky, E. R. Vance, M. L. Carter, B. Ebbinghaus, O. Krikorian, J. Lian, L. M. Wang, and J. G. Catalano, "Enthalpies of Formation of Ce-Pyrochlore, $Ca_{0.93}Ce_{1.00}Ti_{2.035}O_{7.00}$, U-Pyrochlore, $Ca_{1.46}U_{0.234}{+}U_{0.466}{+}Ti_{1.85}O_{7.00}$ and Gd-Pyrochlore, $Gd_2Ti_2O_7$: Three Materials Relevant to the Proposed Waste Form for Excess Weapons Plutonium," *J. Nucl. Mater*., **303** [2–3] 226–39 (2002).

[28]N. U. Navi, R. Z. Shneck, T. Y. Shvareva, G. Kimmel, J. Zabicky, M. H. Mintz, and A. Navrotsky, "Thermochemistry of $(Ca_xSr_{1-x})TiO_3$, $(Ba_xSr_{1-x})TiO_3$, and $(Ba_xCa_{1-x})TiO_3$ Perovskite Solid Solutions," *J. Am. Ceram. Soc*., **95** [5] 1717–26 (2012).

[29]O. Kubaschewski and C. B. Alcock, *Metallurgical Thermochemistry*. p. 462, Pergamon Press, London, 1979.

[30]H. Kojitani, A. Navrotsky, and M. Akaogi, "Calorimetric Study of Perovskite Solid Solutions in the $CaSiO_3$–$CaGeO_3$ System," *Phys. Chem. Miner*., **28** [6] 413–20 (2001).

[31]R. I. Eglitis, "*Ab Initio* Calculations of $SrTiO_3$, $BaTiO_3$, $PbTiO_3$, $CaTiO_3$ and $BaZrO_3$ (001) and (011) Surfaces," *Integr. Ferroelectr*., **108**, 11–20 (2009).

[32]G. Z. Wang, C. R. Li, J. Cui, and Z. Y. Man, "*Ab Initio* Study of $ATiO_3$ (001) Surfaces," *Surf. Interface Anal*., **41** [12–13] 918–23 (2009).

[33]S. P. Chen, "Compositional and Physical Changes on Perovskite Crystal Surfaces," *J. Mater. Res*., **13** [7] 1848–52 (1998).

[34]Y. X. Wang, M. Arai, T. Sasaki, and C. L. Wang, "First-Principles Study of the (001) Surface of Cubic $CaTiO_3$," *Phys. Rev. B*, **73** [3] 035411, 7pp (2006).

[35]R. I. Eglitis and M. Rohlfing, "Comparative *ab Initio* Calculations of $SrTiO_3$ and $CaTiO_3$ Polar (111) Surfaces," *Phys. Status Solidi B*, 1–7 doi: 10.1002/pssc.201248072. (2012).

[36]J. Padilla and D. Vanderbilt, "*Ab Initio* Study of $BaTiO_3$ Surfaces," *Phys. Rev. B*, **56** [3] 1625–31 (1997).

[37]S. Piskunov, E. A. Kotomin, E. Heifets, J. Maier, R. I. Eglitis, and G. Borstel, "Hybrid DFT Calculations of the Atomic and Electronic Structure for ABO_3 Perovskite (001) Surfaces," *Surf. Sci*., **575** [1–2] 75–88 (2005).

[38]E. Heifets, E. A. Kotomin, and J. Maier, "Semi-Empirical Simulations of Surface Relaxation for Perovskite Titanates," *Surf. Sci*., **462** [1–3] 19–35 (2000).

[39]G. C. C. Costa, P. S. Maram, and A. Navrotsky, "Thermodynamics of Nanoscale Lead Titanate and Barium Titanate Perovskites," *J. Am. Ceram. Soc*., **95** [10] 3254–62 (2012).

[40]D. J. Payne, R. G. Egdell, A. Walsh, G. W. Watson, J. Guo, P. A. Glans, T. Learmonth, and K. E. Smith, "Electronic Origins of Structural Distortions in Post-Transition Metal Oxides Experimental and Theoretical Evidence for a Revision of the Lone Pair Model," *Phys. Rev. Lett*., **96** [15] 157403, 4 pp (2006).

[41]Y. Y. Ma, R. H. R. Castro, W. Zhou, and A. Navrotsky, "Surface Enthalpy and Enthalpy of Water Adsorption of Nanocrystalline Tin Dioxide: Thermodynamic Insight on the Sensing Activity," *J. Mater. Res*., **26** [7] 848–53 (2011).

[42]E. Takayama-Muromachi and A. Navrotsky, "Energetics of Compounds ($A^{2+}B^{4+}O_3$) with the Perovskite Structure," *J. Solid State Chem*., **72** [2] 244–56 (1988).

[43]R. D. Shannon and C. T. Prewitt, "Effective Ionic Radii in Oxides and Fluorides," *Acta Crystallogr. Sect. B: Struct. Sci*., **25**, 925–46 (1969). □